

THE EXCITATION OF N₂H⁺ IN INTERSTELLAR MOLECULAR CLOUDS. I - MODELS

F. DANIEL^{1,2}, J. CERNICHARO¹, M.-L. DUBERNET²

Draft version 20th September 2018

Abstract

We present LVG and non-local radiative transfer calculations involving the rotational and hyperfine structure of the spectrum of N₂H⁺ with collisional rate coefficients recently derived by us. The goal of this study is to check the validity of the assumptions made to treat the hyperfine structure and to study the physical mechanisms leading to the observed hyperfine anomalies.

We find that the usual hypothesis of identical excitation temperatures for all hyperfine components of the $J=1-0$ transition is not correct within the range of densities existing in cold dense cores, i.e., a few $10^4 < n(\text{H}_2) < \text{a few } 10^6 \text{ cm}^{-3}$. This is due to different radiative trapping effects in the hyperfine components. Moreover, within this range of densities and considering the typical abundance of N₂H⁺, the total opacity of rotational lines has to be derived taking into account the hyperfine structure. The error made when only considering the rotational energy structure can be as large as 100%.

Using non-local models we find that, due to saturation, hyperfine anomalies appear as soon as the total opacity of the $J=1-0$ transition becomes larger than $\simeq 20$. Radiative scattering in less dense regions enhance these anomalies, and particularly, induce a differential increase of the excitation temperatures of the hyperfine components. This process is more effective for the transitions with the highest opacities for which emerging intensities are also reduced by self-absorption effects. These effects are not as critical as in HCO⁺ or HCN, but should be taken into account when interpreting the spatial extent of the N₂H⁺ emission in dark clouds.

Subject headings: line: formation : profiles — molecular processes — radiative transfer — ISM: clouds : molecules : abundances

1. INTRODUCTION

N₂H⁺ was one of the first molecular ions detected in interstellar space (Thaddeus & Turner 1975). The $J=1-0$ line of this species has been extensively observed toward cold dark clouds and protostellar cores to get some estimates of the physical conditions of the gas (see, e.g., Bergin et al. (2002); Tafalla et al. (2004); Hotzel et al. (2004); Belloche & André (2004); Caselli et al. (2002)). These observations indicate that N₂H⁺ is a good tracer of the highest density regions of dark clouds. It seems that N₂H⁺ is less depleted onto dust grain surfaces than CO and other molecular species. This is probably related to the fact that N₂, the chemical mother species of N₂H⁺, is more volatile and condensates at lower temperatures than carbon monoxide. In addition, the complex hyperfine structure of N₂H⁺ increases the odds to have at least one optically thin hyperfine line component to probe the innermost regions of these clouds. Therefore, this species is in principle an interesting tool to study cold dark clouds. However, a drawback has been the lack of collisional rate coefficients between N₂H⁺ and molecular hydrogen (or helium). The observational data indicate some hyperfine intensity anomalies that could be due to selective collisional processes or to radiative transfer effects (see González-Alfonso & Cernicharo (1993) for the case the analogous case of HCN hyperfine intensities in dark clouds).

For current research, it is clear that astronomers need

to know the state to state collisional rates of N₂H⁺ with H₂ and He. This will be even more necessary for ALMA due to the much higher angular resolution and higher sensitivity observations that it could provide of protostellar cores in several rotational transitions of N₂H⁺ (up to $J=9-8$).

N₂H⁺ has also been detected in warm molecular clouds (e.g. Turner & Thaddeus (1977)) where the lines are broader and very strong. In these objects only the hyperfine structure due to the external N-atom could be noticed as the splitting produced by the internal N-atom is lower than the intrinsic line width. Nevertheless, in order to correctly model the N₂H⁺ intensities emerging from these clouds, astronomers need a complete set of state to state collisional rate coefficients for high temperatures.

A detailed study on molecular ions excitation was carried out by Green (1975) and a set of collisional rate coefficients for N₂H⁺ colliding with He was provided. In that work, the rate coefficients were given for transitions among N₂H⁺ rotational energy levels. Recently, Daniel et al. (2005) extended the previous study by computing a new set of collisional rate coefficients for transitions among hyperfine energy levels and using a new potential energy surface. The range of kinetic temperatures is between 5-50 K and in a future paper, rate coefficients for temperatures up to 300 K will be provided.

The paper is organized as follows: Section 2 is devoted to the spectroscopy of N₂H⁺. In section 3 we present the results obtained with a Large Velocity Gradient (LVG) model to discuss the treatment of molecular hyperfine transitions. Comparisons with the cases of HCN and HCl are made. In section 4 we present results from non-local radiative transfer models applied to N₂H⁺ for different

Electronic address: daniel@damir.iem.csic.es, cerni@damir.iem.csic.es, mldubernet@damir.iem.csic.es

¹ Dept. Molecular and Infrared Astrophysics (DAMIR), Consejo Superior de Investigaciones Científicas (CSIC), C/ Serrano 121, 28006 Madrid, Spain

² Observatoire de Paris-Meudon, LERMA UMR CNRS 8112, 5, Place Jules Janssen, F-92195 Meudon Cedex, France.

cloud structures.

2. SPECTROSCOPY OF N_2H^+

The energy levels of N_2H^+ are characterized by the quantum numbers J (rotational quantum number), F_1 that results from the coupling of \hat{J} with \hat{I}_1 ($\hat{F}_1 = \hat{J} + \hat{I}_1$, where $I_1=1$ corresponds to the nuclear spin of the outer nitrogen), and F ($\hat{F} = \hat{F}_1 + \hat{I}_2$, where $I_2=1$ for the inner nitrogen). We have maintained the symbols used in Daniel et al. (2004, 2005), except for J . The external nitrogen nucleus induces the largest splitting since its coupling constants are larger than those of the internal nucleus. Following Gordy & Cook (1984), the hyperfine energy levels can be found by diagonalizing the molecular Hamiltonian $H_{mol} = B\hat{J}^2 - D\hat{J}^4 + H_{coupling}$, where B and D are respectively the rotational and centrifugal distortion constants of the molecule and $H_{coupling}$ the effective nuclear coupling Hamiltonian. The Einstein coefficients ($A_{u \rightarrow l}$) are given by the equation:

$$A_{JF_1F \rightarrow J'F'_1F'} = \frac{64\pi^4}{2hc^3} \mu^2 \nu_{JF_1F \rightarrow J'F'_1F'}^3 \times \frac{J'}{[F]} S_{JF_1F \rightarrow J'F'_1F'}(\nu)$$

with the line strengths given by:

$$S_{JF_1F \rightarrow J'F'_1F'} = [F_1 F'_1 F F'] \left\{ \begin{matrix} J & F_1 & I_1 \\ F'_1 & J' & 1 \end{matrix} \right\}^2 \left\{ \begin{matrix} F_1 & F & I_2 \\ F'_1 & F'_1 & 1 \end{matrix} \right\}^2 (2)$$

where $[x]$ stands for $(2x+1)$ and $\left\{ \begin{matrix} \cdot & \cdot & \cdot \\ \cdot & \cdot & \cdot \end{matrix} \right\}$ is the Wigner-6j coefficient. The values adopted for rotational and coupling constants were provided by L. Dore (see Daniel et al. (2004)) and where determined following the method described in Caselli et al. (1995). We assume a dipole moment for N_2H^+ of 3.4 ± 0.2 D, as derived experimentally by Havenith et al. (1990). It is in excellent agreement with the value of 3.37 D derived theoretically by Botschwina (1984). The resulting frequencies and line strengths for the $J=1-0$ transition are given in Table 1. Figure 2 shows energy diagrams of the $J=1$ and $J=0$ hyperfine levels and indicates the line strengths of the hyperfine transitions. Figure 1 shows the $J=1-0$ hyperfine components together with their labeling.

Due to hyperfine interactions, there are 9 distinct energy levels for $J > 1$, 7 for $J=1$ and 3 for $J=0$. It is worth noting that the three energy levels in $J=0$ are indistinguishable from a spectroscopic point of view, as their energy splitting is less than 10^{-6} Hz. Thus, although there are actually 15 allowed hyperfine transitions connecting $J=1$ to $J=0$, there are only 7 resolved features, usually labeled as: 110-011, 112-012 (112-011, and 012), 111-010 (111-010, 011, and 012), 122-011 (122-011 and 012), 123-012, 121-011 (121-010, 011, and 012), and 101-012 (101-010, 011 and 012). Hereafter, we call hyperfine component each one of 15 transitions, and set of transitions is used to refer to each group among the seven groups of blended components, using the labeling indicated above.

3. LVG MODELS

3.1. Effect of collisional rate coefficients

To date, two sets of collisional rates are available for the rotational structure of N_2H^+ : Green (1975) and

Daniel et al. (2005)³. The differences between state to state rate coefficients increase with both ΔJ and J as discussed in Daniel et al. (2005). In Figure 3 are compared opacities and excitation temperatures obtained using the two different sets in the same LVG code. There is agreement within a few percent, and the main differences are mainly due to changes in critical densities. At 10 K, the rate coefficients for $\Delta J = 1$ agree within 20% and the critical densities for the radiative lines differ by a similar factor in the opposite way. In particular, the rate coefficient for the transition $J=1-0$ is 22% higher using the results of Daniel et al. (2005) and the derived critical density is 22% smaller. In other words, the recently derived rate coefficients make this transition thermalized at slightly lower densities.

For densities below 10^4 cm^{-3} the excitation temperature of the $J=1-0$ line would be very close to the cosmic background temperature due to the high dipole moment of N_2H^+ and the high critical densities (see Figure 3). However, for column densities as low as 10^{12} cm^{-2} (left panels of Figure 3), the opacity of the $J=1-0$ and $J=2-1$ lines would be large enough to produce significant absorption effects on the radiation emerging from the inner and denser regions of the clouds. It is difficult to estimate from emission measurements the abundance of N_2H^+ in these low density regions. However, by observing the $J=2-1$ and $J=3-2$ lines it could be possible to assess the effect of the external layers of the cloud on the emerging profiles of the low- J lines of N_2H^+ , and thus to indirectly determine the spatial repartition in N_2H^+ abundance. This effect will be discussed in detail below.

3.2. LVG treatment of hyperfine transitions

The LVG model used for the simulations presented in this work takes into account all possible collisional and radiative transitions among hyperfine levels. Nevertheless, it does not account for local overlap, and particularly, the 15 transitions associated with $J=1-0$ line are treated independently. In order to check the effect of the hyperfine structure, we performed calculations with and without it for three species: HCl, HCN and N_2H^+ . Figure 4 shows, for the three species, the ratio of the summed opacities of the hyperfine components, $\tau(1-0) = \sum \tau_i$, to the opacity of the unsplitted rotational transition, $\tau_R(1-0)$. This ratio will be referred to as $R_\tau = \tau(1-0)/\tau_R(1-0)$. The range of $\tau(1-0)$ explored is 0.1 to 100. This figure reveals differences between the two approaches. Under LTE conditions (large volume density), or in radiative equilibrium with the cosmic radiation background (low volume density), the two approaches lead to the same estimate of the total opacity because under these conditions the hyperfine levels are populated according to the statistical weights :

$$n_{JF_1F} = \frac{[F]}{[J I_1 I_2]} n_J \quad (3)$$

³ It was incorrectly stated, in Daniel et al. (2004, 2005) that the potential energy surface (PES) used by Green (1975) was calculated under the electron-gas approximation. Indeed, as explained in Green (1975), the PES was determined using the self-consistent field approach which gives accurate results for interacting systems where the charge-induced dipole term is prominent. This is actually the case for the N_2H^+ - He system and explain the agreement between the two sets of collisional rate coefficients for the transitions among the first rotational levels.

where $[JI_1I_2]$ is the total number of hyperfine sub-magnetic levels for a given rotational quantum number J . Such a population scheme of hyperfine energy levels occurs when lines are optically thin or in the domains of low and high volume densities, as Einstein ($A_{u \rightarrow l}$) and collisional ($C_{u \rightarrow l}$) rate coefficients reduce similarly after summation over initial and final hyperfine levels:

$$\sum_{F_1 F'_1 F F'} [F] C_{JF_1 F \rightarrow J' F'_1 F'} = [JI_1I_2] C_{J \rightarrow J'} \quad (4)$$

$$\sum_{F_1 F'_1 F F'} [F] A_{JF_1 F \rightarrow J' F'_1 F'} = [JI_1I_2] A_{J \rightarrow J'} \quad (5)$$

If $n(\text{H}_2) \sim A_{J \rightarrow J'} / C_{J \rightarrow J'}$, both collisional and radiative processes compete in populating the energy levels. Figure 4 shows that in this case the excitation processes are less effective to populate the first excited rotational levels if the hyperfine structure is considered. Thus, the total population of the fundamental level $J=0$ is underestimated in a treatment that only includes the rotational molecular structure. It gives rise to an underestimation of the opacity of the $J=1-0$ and $J=2-1$ lines, and to an overestimate of the opacity of the $J=3-2$ transition of N_2H^+ and HCN . For HCl there is always an overestimate of the opacity.

When the hyperfine structure is taken into account, both Einstein and collisional rate coefficients have the same order of magnitude than the corresponding values for the rotational structure. Thus, the amount of radiative de-excitation, in the hyperfine description, is globally larger for the rotational lines. Then, this makes R_τ increase with the total opacity of the lines. As opacity increases, the different Einstein coefficients of hyperfine lines lead to different excitation conditions for each hyperfine component, i.e., different excitation temperatures (see Figure 7). In addition, in an inhomogeneous cloud, hyperfine lines may be excited in regions where other lines still have low excitation temperatures. This effect is analyzed in section 4 with the help of non-local radiative transfer models.

HCl behaves differently with respect to HCN and N_2H^+ due to its large rotational constant ($B \sim 313.0$ GHz). The first excited levels are hardly populated at low temperatures. We can roughly estimate the number of rotational levels reached by collisions to be $\sim k_B T / hB$. Thus, for HCl , most molecules are in the fundamental $J=0$ level for $T_K=10$ K and $R_\tau \simeq 1$. Although some discrepancies do appear for R_τ in high- J transitions, the opacities of these lines are so low at $T_K=10$ K that the emerging intensity is negligible. At low temperatures, a hyperfine treatment of HCl is thus not necessary.

HCN and N_2H^+ have similar rotational constants (44.3 GHz and 46.6 GHz respectively). For these two species, the excited rotational levels are efficiently pumped by both collisions and radiation. Hence, the hyperfine structure has to be considered to correctly derive column densities and abundances. For the $J=1-0$ transition of N_2H^+ the error induced in the opacity estimate by neglecting the hyperfine structure varies from 20% ($\tau \sim 1$) to 100% ($\tau \sim 100$).

3.3. $J=1-0$ Hyperfine Brightness Temperature Ratios

Hereafter, we call T_{ex}^i the excitation temperature of the hyperfine component i . LVG calculations show that

there are two domains in the estimate of T_{ex}^i for $J=1-0$. When opacities of individual components are low ($\tau_i \ll 1$), the excitation temperature is the same for all hyperfine components. In this case, the opacities are proportional to line strengths s_i : $\tau_i = s_i \tau (1 - 0)$. This behavior is similar to what is expected in the LTE regime. For higher opacities, photon trapping induces different behaviors for the hyperfine components.

In the LTE approximation, where T_{ex} is assumed to be the same for all lines, the brightness temperature ratios vary monotonously with the rotational line opacity:

$$\frac{T_B^{i*}}{T_B^{j*}} = \frac{1 - e^{-\tau_i}}{1 - e^{-\tau_j}} \quad (6)$$

Therefore, the brightness temperature ratios will change from the optically thin case, where they are given by the statistical weights $1 : 3 : 5 : 7$, to unity in the optically thick case. Figure 5 shows the hyperfine ratios, in LTE and non-LTE conditions, of the different hyperfine transitions with respect to the thickest one, i.e., $JF_1F=123-012$. As expected for high densities, the LVG calculations are coincident with the result of the LTE approximation. The LVG calculations show that in a large domain of the $(n(\text{H}_2), N(\text{N}_2\text{H}^+))$ plane, i.e. $n(\text{H}_2) < 10^6 \text{ cm}^{-3}$ and $N(\text{N}_2\text{H}^+) > 10^{12} \text{ cm}^{-2} / (\text{km s}^{-1} \text{ pc}^{-1})$, the ratios are smaller than expected in the LTE approximation. Furthermore, ratios below the lower possible limit predicted under LTE conditions, i.e. $1/7, 3/7, 5/7$, occur when hyperfine levels are not populated according to their statistical weights. Hence, fitting observational data using the hypothesis of identical excitation temperatures for all $J=1-0$ hyperfine components will lead to an erroneous determination of the total opacity. From our calculations it seems that using this procedure underestimates $\tau(1-0)$.

To discuss the behavior of the ratios, it is convenient to define an averaged excitation temperature, T_{ave} , using LVG results for individual rotational lines, and their hyperfine components, as:

$$T_{ave} = T_0 / \ln \left(1 + \frac{T_0 \cdot \sum \tau_i}{\sum \tau_i \cdot J_{\nu_i}(T_{ex}^i)} \right) \quad (7)$$

with $T_0 = h\nu/k_B$ and $\tau(1-0) = \sum \tau_i$.

Figure 6 shows the LVG excitation temperature for all hyperfine components of the $J=1-0$ transition divided by T_{ave} . This figure also shows the ratio of individual hyperfine line opacities to the expected LTE opacities. Figure 7 shows individual excitation temperatures and opacities for all hyperfine transitions. It is clear from these figures that the effects are only important for large column densities, i.e., for large total opacities as discussed above. Non-LTE effects tend to reduce the spread of the opacities of the different lines transferring opacity from the thickest to the thinnest ones. For the hyperfine transitions associated to $J=1-0$, and from Figures 6 and 7, we find the following trends:

- for $JF_1F=123-012$: $T_{ex}^i > T_{ave}$ and $\tau_i < s_i \tau (1-0)$
- for lines with initial quantum number $F=2$: $T_{ex}^i \sim T_{ave}$ and $\tau_i \sim s_i \tau (1-0)$
- for lines with initial quantum number $F=1$ or $F=0$: $T_{ex}^i < T_{ave}$ and $\tau_i > s_i \tau (1-0)$

We note that the variations of excitation temperatures and opacities for the different hyperfine components are anti-correlated, i.e., an increase of T_{ex}^i is accompanied by a decrease of τ_i , and inversely (see Figure 6). This fact suggests that non-LTE effects mainly induce variations in the population of the $JF_1F=012$ level (the lower energy level in the reference hyperfine transition) compared to the LTE values. As for moderate and large opacities the brightness temperatures T_B^* , are less sensitive than T_{ex}^i to variations in τ_i , the non-LTE effects tend to increase T_B^* for the $JF_1F=123-012$ line and induce a decrease of T_B^* for lines with initial quantum number $F=0$ or $F=1$. Thus, for a given H_2 density and N_2H^+ abundance, ratios derived in the LVG approximation are smaller than those obtained under the LTE approximation (see Figure 5).

4. NON-LOCAL RADIATIVE TRANSFER FOR N_2H^+

The LVG calculations discussed in the previous section could be a reasonable approximation to the emerging N_2H^+ intensities from dark clouds when line opacities are low. However, as the line strengths of the hyperfine components are different, the density structure of the cloud, radiation scattering and/or radiative coupling between different cloud regions could affect the population of N_2H^+ energy levels. In order to check the validity of the LVG approximation and the different assumptions made earlier in this paper to interpret the N_2H^+ $J=1-0$ transition, we carried out non-local calculations using the code developed and described by González-Alfonso & Cernicharo (1993). For the opacity range considered in this work the code provides reliable and fast convergence.

We assume a cloud at 160 pc with an angular diameter of $30''$ which corresponds to a radius of $3.6 \cdot 10^{16}$ cm (i.e. 0.023 pc), and we consider three different sets of models. In the first one we consider a core of uniform density. In the second set the central core is surrounded by an envelope with size 3 and 6 times the core size. Finally, the last set corresponds to a collapsing cloud. In all models the turbulence velocity was varied from 0 to 0.4 km s^{-1} by step of 0.1 km s^{-1} . Finally, we adopt a kinetic temperature of 10 K in all models.

In all figures related to this section the ordinate scale is antenna temperature obtained by convolving the cloud brightness temperature with the beam of the 30-m IRAM radio telescope as follows: half power beam widths of $27''$, $13.5''$ and $9''$, beam efficiencies of 0.76, 0.59 and 0.42, and error beams of $350''$, $220''$, and $160''$ for the $J=1-0$, $2-1$ and $3-2$ lines respectively. The error beam is always larger than the size of the dense regions and thus the energy entering the telescope radiation pattern through the error beam just accounts for a few percent of the total intensity at most. Moreover, the contribution to $J=1-0$ from the extended envelopes surrounding the cores is fully taken into account by considering the convolution with the beam of the telescope (main beam and error lobe). The only plots for which the emerging intensity has not been convolved with the beam correspond to the two lowest right panels of Figure 10. In these cases, we aim to show the influence of the high density region on the excitation of the molecules in the low density envelope and this would have been hidden by performing the convolution with the telescope beam pattern.

4.1. Uniform density cores

For this set of models the N_2H^+ abundance has been varied from $4 \cdot 10^{-10}$ to $6.4 \cdot 10^{-9}$, and the volume density from $2.5 \cdot 10^4 \text{ cm}^{-3}$ to $4 \cdot 10^5 \text{ cm}^{-3}$, by multiplicative steps of 4. Figure 8 shows the emerging line profiles for the $J=1-0$, $2-1$ and $3-2$ transitions for all computed densities $n(H_2)$ and abundances $X(N_2H^+)$. As expected, the brightness temperature increases with $n(H_2)$ due to collisional excitation, leading to the thermalization of the the $J=1-0$ hyperfine components. We see that the brightness temperatures of the $J=1-0$, $2-1$, and $3-2$ transitions are more sensitive to a variation of $n(H_2)$ in the range $2.5 \cdot 10^4 \text{ cm}^{-3} < n(H_2) < 4 \cdot 10^5 \text{ cm}^{-3}$ than to an increase of $X(N_2H^+)$. This can be understood by looking at figure 7: in this range of $n(H_2)$ the excitation temperatures increase rapidly. Moreover, for $J=1-0$ total opacities below 20, the excitation temperatures depend essentially on the volume density as radiative trapping effects are negligible and do not induce significant departure for the different T_{ex}^i from a single value. Consequently, in the optically thin case and for a given volume density, the line intensities are proportional to $X(N_2H^+)$ (raw corresponding to $n(H_2) = 2.5 \cdot 10^4 \text{ cm}^{-3}$ on Figure 8). Radiative trapping and line saturation only become important for large N_2H^+ column densities. On Figure 8, for the $J=1-0$ line, and on the panel corresponding to $n(H_2)=10^5 \text{ cm}^{-3}$, we see that increasing the abundance from $1.6 \cdot 10^{-9}$ to $6.4 \cdot 10^{-9}$ modify the ratio between the the $JF_1F = 101-012$ and $121-011$ sets of transitions. This change is due to radiative trapping and entails variations in the T_{ex}^i for the involved hyperfine components. Thus for large opacities, i.e. $\tau(1-0) \sim 20$, the excitation temperatures start to be sensitive to $X(N_2H^+)$.

One of the main results that can be derived from Figure 8 is that hyperfine intensity anomalies appear when increasing the N_2H^+ abundance. This is similar to the effect found in HCN and discussed by González-Alfonso & Cernicharo (1993). For total opacities in the $J=1-0$ transition above 10, differential radiative trapping across the cloud starts to affect the relative intensities of the hyperfine components. Moreover, in an inhomogeneous cloud we could expect to be sensitive to different spatial extents for each hyperfine component (see Cernicharo & Guélin (1987); González-Alfonso & Cernicharo (1993)). This is even more striking when considering transitions with the same initial quantum number F , expected to have the same brightness temperature in the LTE limit. The most affected hyperfine set of components is the $121-011$ set which indeed appears weaker than the $101-012$ and $111-010$ sets (see section 2). A low brightness temperature for this set has already been observed (see e.g. Lee et al. (1999); Caselli et al. (1995)). We find the general trend $T_B(111-010) \gtrsim T_B(101-012) > T_B(121-011)$ and $T_B(112-012) \gtrsim T_B(122-011)$. This behavior originates from differential non-LTE effects in the hyperfine components of the $J=0$ $F_1=1$ levels ($F=0,1,2$). This is not surprising as the three transitions from $J=1$ $F=1$ ($F_1=0,1,2$) have different line strengths (see Table 1). The $121-011$ transition mostly depends on the $JF_1F=010$ level and is independent of $JF_1F=012$ while the $111-010$ and $101-012$ sets mainly depend on $JF_1F=012$. Thus, the $121-011$ set weakness compared to the other two must be related

to an underpopulation of the $JF_1F=012$ level that produces higher excitation temperatures for the hyperfine lines involving it. As shown in Figure 8 the effect appears for high abundances, i.e., large opacities, while for low abundances the three sets have the same intensities. Hence, it seems that it is not related to a collisional effect but to a radiative one. The sum of the line strengths for lines connecting the $J=1$ to the $J=0$ level is larger for $JF_1F=012$ than for the others. Thus, for large opacities this level will be more affected by radiative trapping than the others.

For the $J=2-1$ and $J=3-2$ lines the effect of the abundance on the hyperfine intensities is similar. Large abundances lead to larger opacities, differential radiative trapping between the hyperfine components, and to anomalies in the observed line intensities. For these levels, line overlap is really important as the hyperfine components are closer in frequency and should be taken into account in a detailed modeling. In collapsing clouds the velocity field could allow to have radiative coupling across the cloud between hyperfine components with different frequencies. This effect has been found to be extremely important in molecules such as HCN (G3n3lez-Alfonso & Cernicharo 1993). In the models shown in Figure 8 we only consider the effects of opacity for each line without taking into account population transfer between levels due to radiative connection between them. Hence, the effects shown in this figure for large abundances are purely due to the line opacities. For the $J=2-1$ and $3-2$ lines, the self absorption induced by the external layers of the cloud is extremely important. When mapping clouds, the $J=2-1$ and $3-2$ transitions have little intensity outside the central position. However, although the excitation temperature of their hyperfine components could be low for offset positions, their line opacities are still large enough to produce significant effects on the emerging profiles toward the densest regions. For example, the model in Figure 8 with $n(\text{H}_2) = 2.5 \cdot 10^4 \text{ cm}^{-3}$ has low emission for all lines. However, the opacities are large enough for the strongest hyperfine components of the $J=1-0$ and $J=2-1$ lines to produce the above mentioned effects. Figure 9 shows the opacities of the lines for $n(\text{H}_2)=10^5 \text{ cm}^{-3}$ which roughly agree with those found in the case $n(\text{H}_2)=2.5 \cdot 10^4 \text{ cm}^{-3}$ multiplied by a factor 4. We see that the opacity of $J=2-1$ will be even larger than that of $J=1-0$, and of the order of 0.75/7.5 for the strongest component and for the lowest/largest abundance of N_2H^+ . As shown in Figure 7 the excitation temperatures of the $J=1-0$ hyperfine components vary strongly in the range $10^4 < n(\text{H}_2) < 10^6 \text{ cm}^{-3}$. The same will occur for the $J=2-1$ and $3-2$ hyperfine components. Consequently, strong absorption will be produced in the low density layers of a cloud with a marked density structure.

4.2. Core/Envelope Clouds

We have finally explored more complex structures for the cloud to check the effects quoted above. Figure 10 shows the results for two different cases. Left and central panels correspond to a simple core+envelope structure. For the line profiles shown in the left panels ($T_K=10 \text{ K}$, $n(\text{H}_2)_{\text{core}} = 4 \cdot 10^5 \text{ cm}^{-3}$, $n(\text{H}_2)_{\text{env}}=4 \cdot 10^4 \text{ cm}^{-3}$, $X(\text{N}_2\text{H}^+)_{\text{core/env}}=4 \cdot 10^{-10}$, $R_{\text{core}}=3.6 \cdot 10^{16} \text{ cm}$, $R_{\text{env}}=2 R_{\text{core}}$), the opacity in the envelope for the $J=1-$

0 line is very small. The emerging profile is practically coincident with the one arising from the core. However, the $J=2-1$ line is optically thick in the envelope and important absorption is caused to the emission from the core. As the opacity of the different hyperfine components depends on the line strength, weak lines are not affected (components at extreme negative and positive velocities), while the central components are much more affected. The $J=3-2$ lines are practically not affected by the envelope.

A different situation occurs if the abundance of N_2H^+ and/or the physical size of the envelope increase. The line profiles reported in the central panels of Figure 10 ($T_K=10 \text{ K}$, $n(\text{H}_2)_{\text{core}} = 4 \cdot 10^5 \text{ cm}^{-3}$, $n(\text{H}_2)_{\text{env}}=5 \cdot 10^3 \text{ cm}^{-3}$, $X(\text{N}_2\text{H}^+)_{\text{core/env}}=6.4 \cdot 10^{-9}$, $R_{\text{core}}=3.6 \cdot 10^{16} \text{ cm}$, $R_{\text{env}}=6 R_{\text{core}}$) show that the strongest hyperfine components of the $J=1-0$ line are strongly affected by absorption (the effect is similar to the one obtained in the models shown in the previous section, see Figure 8, where absorption occurs in the most external core layers where the excitation temperature has decreased with respect to the center). For the $J=2-1$ hyperfine lines the presence of the envelope affect dramatically the emerging intensities and the shape of the line. The $J=3-2$ line is less affected since the density in the envelope is not large enough to pump the $J=2$ and $J=3$ levels efficiently. The core also has an effect on the excitation temperatures of the N_2H^+ lines in the envelope. The right panels of Figure 10 show the emerging profile from the envelope at a position located $30''$ away from the center. The top right panel shows the comparison of the emission from the envelope alone and the emission obtained when the core is also present and excites radiatively the N_2H^+ molecules of the envelope. The intensity of the $J=1-0$ line has increased by a factor ~ 2 . The other two right panels show the radial intensity distribution (not convolved with the telescope beam) for the $J=1-0$ and $J=2-1$ lines (integrated intensity over all hyperfine components). The "heating effect" is clearly seen as a significant increase of the integrated line intensity even at distances of 3-4 times the radius of the core. These effects should be taken into account when interpreting the radial distribution of N_2H^+ from observations of the $J=1-0$ line (which is much easier to detect than the high- J lines in these low density regions).

4.3. Collapsing Clouds

Over the past decades, mm continuum observations and star count analysis (Ward-Thompson et al. 1994) have revealed that the density structure of cold dark clouds consists of an inner region of nearly uniform density and of an outer region where the density decreases as r^{-p} with $p \sim 2.0-2.5$. In this section, we use this type of density profile with a power law index $p = 2$ in order to test the influence of the velocity field on emerging spectra. Figure 11 shows the profiles of the $J=1-0$, $2-1$ and $3-2$ lines for a $180''$ diameter cloud (at a distance $D = 160 \text{ pc}$) with $n_0 = 4 \cdot 10^5 \text{ cm}^{-3}$, $r_0 = 20''$ and a uniform abundance $X(\text{N}_2\text{H}^+) = 2 \cdot 10^{-10}$. The velocity fields compared are linear functions of r with slopes of $\pm 1.5 \text{ km s}^{-1} \text{ pc}^{-1}$ (the velocity at the outer radius is $\pm 0.1 \text{ km s}^{-1}$).

In non-LTE conditions, the line excitation temperatures follow the density profile and, in the present case, decrease outward. Thus, in the case of a linearly de-

creasing velocity field, photons emitted at the center of the cloud appear blue-shifted for the molecules at greater radii which then absorb the red wing of the central emission (the opposite occurs for a linearly increasing velocity field). This effect is important if the lines are optically thick. Thus, in typical interstellar clouds conditions, self absorption affects the $J=2-1$ transition (see figure 9 for the opacities) while the emerging profiles of the $J=1-0$ and $3-2$ lines are similar with and without velocity fields.

On Figure 11, we see that the effect of the infalling material is to enhance the blue wing of the $J=2-1$ central component which is self absorbed in the static model, the red wing of the central component being reduced by self-absorption. In the case of a velocity field linearly increasing with r , the opposite occurs and emission in the red wing is enhanced. Note that because the $J=2-1$ central component is composed of blended hyperfine lines with different line strengths (see figure 11), changes in the line profile are not similar with respect to a change in the sign of the slope.

Also, we stress that this effect is similar to what happens to rotational lines with large opacity, except that, in the present case, the $J=2-1$ central component corresponds to hyperfine blended lines of small intrinsic line width. Thus, characteristic features appear even if the velocity gradient is weak.

4.4. Rate coefficients

In star forming regions, the relatively large abundance of H_2 makes this species the main colliding partner for other molecules. Estimated values of the collisional rate coefficients of molecular species in collision with para- $H_2(j=0)$ can be obtained from the ones calculated with He as the collision partner. The underlying approximation is to consider identical cross sections values for the two colliding systems, and then apply a scaling factor of 1.37 to the rate coefficients in order to correct for the associated different reduced masses. However, by analogy with the results obtained on the collision systems involving HCO^+ , one could expect the cross sections values with H_2 as a collision partner to be 2-3 times larger than those with He depending on the selected rotational transition. As discussed in section 3.1, the main effect introduced by higher collisional rate coefficients is to lower the critical density of the rotational lines, which has direct consequences on the determination of both density and molecular abundance. The hyperfine rate coefficients are also changed through variations of the ratio of the different $P_{jj'}^K$ (see Daniel et al. 2004). Indeed, these variations modify the relative importance of hyperfine rate coefficients among a given rotational line. In order to assess the influence of such variations, we carried out calculations where two distinct approximations are employed to determinate the hyperfine rate coefficients. The first consisted on rate coefficients proportional to the statistical weights of the final levels of the transitions and the second was based on the IOS approximation (see Daniel et al. 2005). Figure 12 shows the emerging profiles resulting from the three sets of calculations for a cloud at $T_K = 10$ K, $n(H_2) = 2 \cdot 10^5 \text{ cm}^{-3}$ and $X(N_2H^+) = 5 \cdot 10^{-10}$. It is readily seen that the relative intensities of $J=1-0$ hyperfine lines are similar and that the largest difference ($\sim 15-20\%$) is encountered for the thickest $JF_1F = 123-012$ line. The three sets give

the same results for the thinnest $JF_1F = 110-011$ line. Moreover, the intensity in the $J=3-2$ line associated with the IOS set of collisional rates is enhanced compared to the two other sets. This is related to the high propensity of the $\Delta F = \Delta F_1 = \Delta J$ transitions which lead to a more efficient pumping of the high- J levels. Note that it entails higher T_{ex} for the $J=2-1$ hyperfine lines which reduce the self-absorption feature in the main $J=2-1$ hyperfine component. Finally, one would expect the collisional rate coefficients calculated with H_2 to affect similarly the intensities in the $J=1-0$ line, through variations of the ratio of the opacity tensors $P_{jj'}^K$. Thus, as discussed above, the most important effect introduced by rate coefficients calculated with H_2 would be to scale all the rate coefficients and thus modify the density and abundance estimates.

5. CONCLUSIONS

We have used numerical methods in order to investigate the excitation properties of molecules with a hyperfine energy structure, focusing specially on N_2H^+ . Our conclusions are summarized as follows :

1. The hyperfine structure must be taken into account in the radiative transfer calculations in order to derive the total amount of molecules present in a given rotational level. When the energy structure of the molecule is restricted to its rotational energy structure, high- J levels are more efficiently populated and the opacities of the low- J transitions are underestimated. The error increases with the column density of N_2H^+ . Errors as large as a factor 2 could be induced if the hyperfine structure of N_2H^+ is neglected.
2. For the typical temperature of dark clouds, i.e. $T_K=10$ K, and $n(H_2) < 10^6 \text{ cm}^{-3}$ the ratio of hyperfine brightness temperatures derived in the LVG approximation are always smaller than the ones predicted using the LTE approximation. Thus, this latter method is inadequate to assess densities or column densities from observed N_2H^+ lines for the typical conditions prevailing in such clouds.
3. The assumption of equal excitation temperatures for all hyperfine components belonging to the same rotational transition is valid for low opacities and fails down for high opacities due to radiative processes. For low opacities, we do not find any difference in the excitation temperatures of the different hyperfine transitions induced by collisional rate coefficients. Our calculations indicate that for temperatures in the range 5-50 K and for all volume densities, the excitation temperature of these lines will be identical if the total opacity of the $J=1-0$ line is small. We stress that such collisional excitation effects, often found in the literature, may not be invoked to explain the intensity anomalies reported for N_2H^+ .
4. Non-local radiative transfer results show that the $J=1-0$ intensity anomalies arise while the opacity of this line increases. Moreover, photon scattering in the low density envelopes affect the $J=1-0$ hyperfine lines differently and tend to reduce the

emerging intensity of the thicker lines whereas the intensity of the thinnest lines is not modified by the envelope. Thus, in order to reproduce the intensities of the $J=1-0$ hyperfine lines, the only valid method is a non-local computation of the radiative transfer.

5. For the typical conditions of cold dark clouds, the $J=2-1$ line is a good probe of low velocity fields. Nevertheless, this transition is difficult to observe from ground based observatories due to the high opacity of the atmosphere at 186 GHz, although some work can be carried out in dry weather conditions.

The authors thank the European Union for support under the FP6 program "The Molecular Uni-

verse" and the Spanish/French Picasso project HF2003-0293. J. Cernicharo would like to thank Spanish MEC for funding support through AYA2003-2785, AYA2000-1784, ESP2001-4516, ESP2002-1627, ESP2002-12407, AYA2003-10113, and ESP2004-00665. Fabien Daniel wishes to thank Spanish MAE-AECI 2004/2005 for a fellowship grant from Program IIa. This study is partly supported by the European Community's human potential Program under contract MCRTN 512302, the "Molecular Universe". We are grateful to A. Spiefieldel, J.R. Pardo and F. Dayou for their help and useful comments concerning the present manuscript.

REFERENCES

- Belloche A., and André P., 2004, *A.&A.*, 419, 35
 Bergin E.A., Alves J., Huard T., Lada C.J., 2002, *ApJ*, 570, L101
 Botschwina P., 1984, *Chem. Phys. Lett.*, 107, 535
 Caselli P., Myers P., Thaddeus P., 1995, *ApJ*, 455, L77
 Caselli P., Benson P.J., Myers P., Tafalla M., 2002, *ApJ*, 572, 238
 Cernicharo J., Guélin M., 1987, *A.&A.*, 176, 299
 Daniel F., Dubernet M.-L. and Meuwly M., 2004, *J. Chem. Phys.*, 121, 4540
 Daniel F., Dubernet M.-L., Meuwly M., Cernicharo J., 2005, *MNRAS*, 363, 1083
 González-Alfonso E., Cernicharo J., 1993, *A.&A.*, 279, 506
 Gordy W. and Cook R.L., *Microwave molecular spectra*, Techniques of chemistry vol 18., Wiley Interscience Publication, 1984
 Green S., 1975, *ApJ*, 201, 366
 Havenith M., Zwart E., Leo Meerts W., ter Meulen J.J., 1990, *J. Chem. Phys.*, 93, 8446
 Hotzel S., Harju J., Walmsley M.C., 2004, *A.&A.*, 415, 1065
 Lee C.W., Myers P.C., Tafalla M., 1999, *ApJ*, 526, 788
 Tafalla M., Myers P.C., Caselli P., Walmsley C.M., 2004, *A.&A.*, 416, 191
 Thaddeus P. and Turner B.E., 1975, *ApJ*, 201, L25
 Turner B.E. and Thaddeus P., 1977, *ApJ*, 211, 755
 Ward-Thompson D., Scott P.F., Hills R.E., André P., 1994, *MNRAS*, 268, 276

$(JF_1F)_u$	$(JF_1F)_l$	Frequency (MHz)	A_{ul} (10^{-5} s^{-1})	s_{ul}
110	011	93171.617	3.628	0.333
112	011	93171.913	0.907	0.417
112	012	93171.913	2.721	1.250
111	010	93172.048	1.209	0.333
111	011	93172.048	0.907	0.250
111	012	93172.048	1.512	0.417
122	011	93173.475	2.721	1.250
122	012	93173.475	0.907	0.417
123	012	93173.772	3.628	2.330
121	010	93173.963	2.015	0.556
121	011	93173.963	1.512	0.417
121	012	93173.963	0.101	0.028
101	010	93176.261	0.403	0.111
101	011	93176.261	1.209	0.333
101	012	93176.261	2.016	0.556

TABLE 1

FREQUENCIES, EINSTEIN COEFFICIENTS (A_{ul}) AND LINE STRENGTHS (s_{ul}) FOR THE HYPERFINE COMPONENTS OF THE $J=1-0$ TRANSITION OF N_2H^+ , AS GIVEN BY EQ. 2 (SEE TEXT). INDEX u (l) DENOTE THE INITIAL (FINAL) LEVELS QUANTUM NUMBERS.

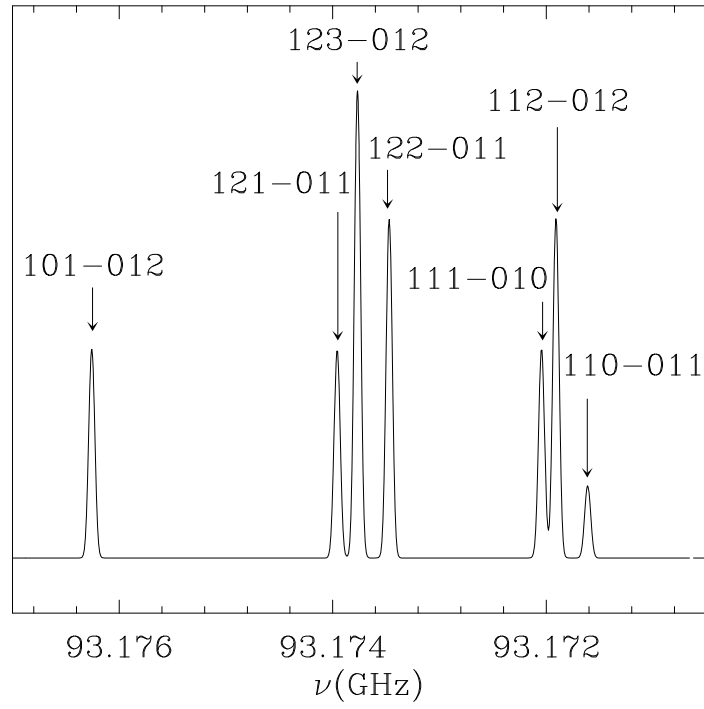


FIG. 1.— Hyperfine transitions associated to $J=1-0$ in the optically thin case. Each resolved frequency is associated to multiple transitions among hyperfine levels (see text), and the standard labeling of the lines is indicated.

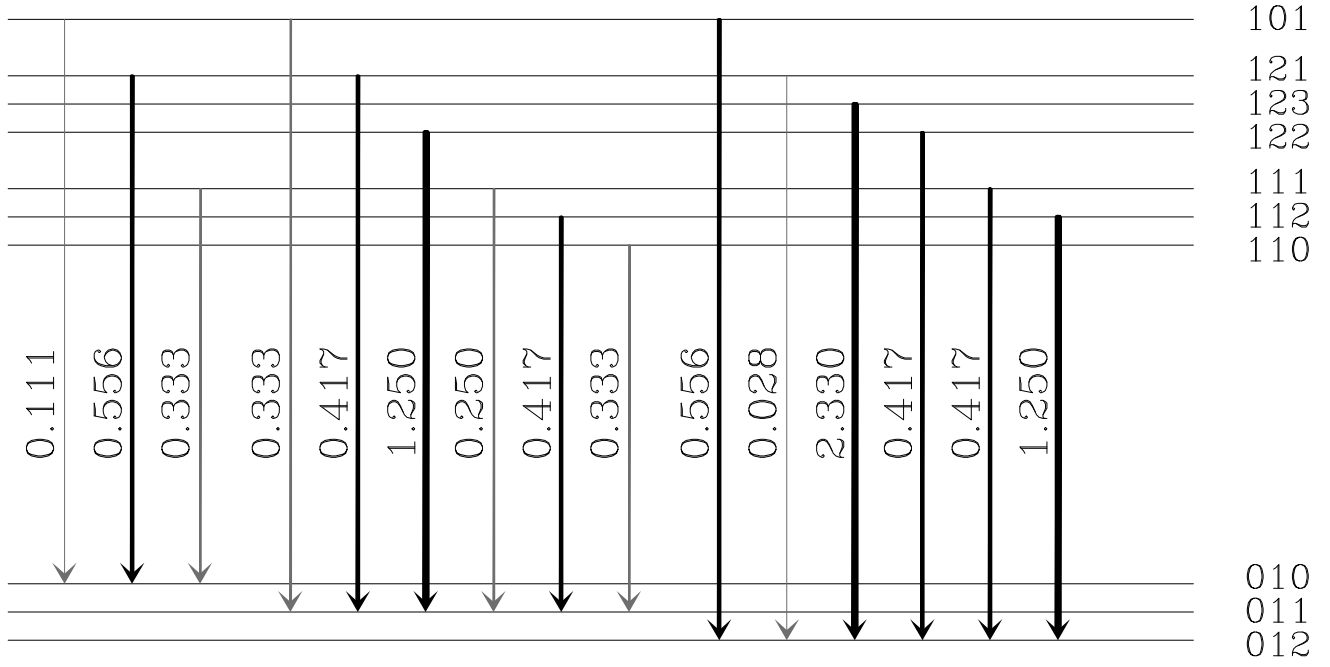


FIG. 2.— Line strengths of the 15 hyperfine components in $J=1-0$ transition. The thickness of the lines indicate their relative weight compared to the others. Lines strengths are normalized in such a way that, summing over all initial $J=1$ levels, gives the degeneracy of the final $J=0$ levels, i.e. 5 for $JF_1F=012$, 3 for $JF_1F=011$ and 1 for $JF_1F=010$. Thus, the sum over all 15 transitions gives the total spin degeneracy.

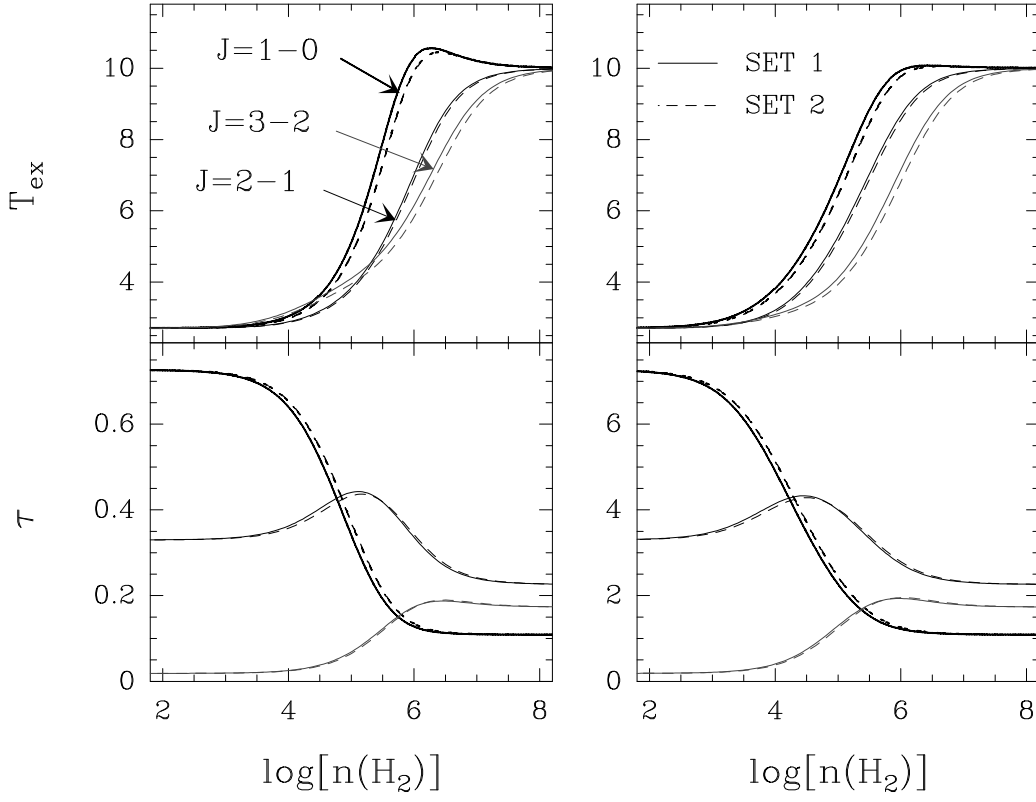


FIG. 3.— Excitation temperatures (T_{ex}) and opacities (τ) obtained with two different sets of collisional rate coefficients and a LVG code, for a temperature of $T = 10 \text{ K}$. SET 1 (solid lines) refers to the latest computed rate coefficients (Daniel et al. 2005) and SET 2 (dashed lines) to the previously available one (Green 1975). Left and right panels correspond to N_2H^+ column densities of respectively 10^{12} and 10^{13} cm^{-2} . A systematic velocity field of 1 km s^{-1} has been assumed for the cloud.

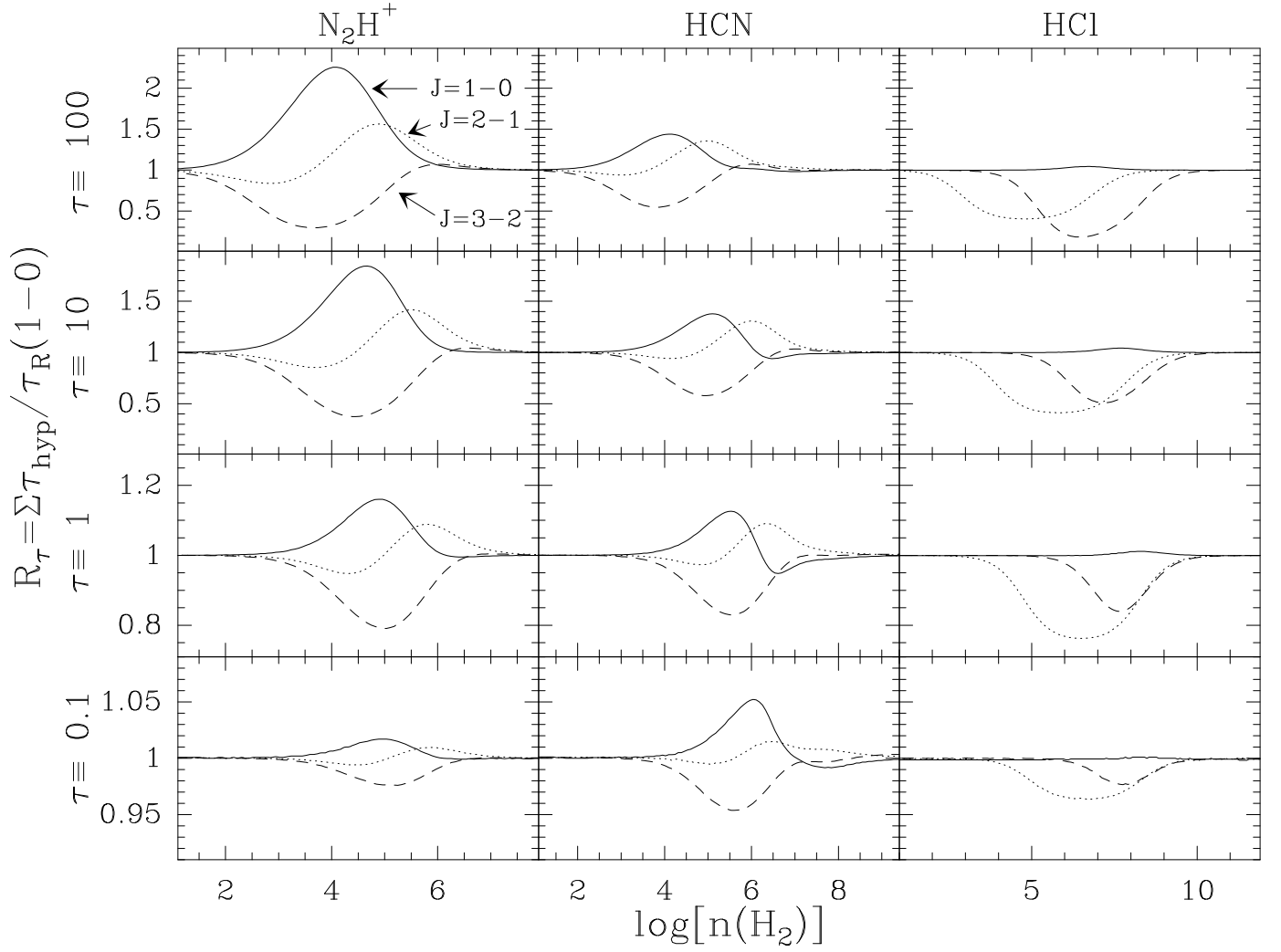


FIG. 4.— Ratio between the opacities of the $J=1-0$ (solid), $J=2-1$ (dotted) and $J=3-2$ (dashed) rotational lines, R_τ , determined with and without hyperfine description for three molecules presenting hyperfine structure: N_2H^+ (left panels), HCN (central panels), and HCl (right panels). For each molecule the column densities are such that, at $T=10\text{K}$, opacities of the $J=1-0$ lines are $\tau(1-0) \sim 0.1, 1, 10$ and 100 . The column densities are respectively: $N(\text{N}_2\text{H}^+) \simeq 2.2 \cdot 10^{11}, 2.3 \cdot 10^{12}, 2.5 \cdot 10^{13}$ and $2.0 \cdot 10^{14} \text{ cm}^{-2}/(\text{km s}^{-1} \text{ pc}^{-1})$; $N(\text{HCN}) \simeq 3.7 \cdot 10^{11}, 3.0 \cdot 10^{12}, 2.5 \cdot 10^{13}$, and $3.4 \cdot 10^{14} \text{ cm}^{-2}/(\text{km s}^{-1} \text{ pc}^{-1})$; $N(\text{HCl}) \simeq 8.5 \cdot 10^{11}, 6.9 \cdot 10^{12}, 7.3 \cdot 10^{13}$, and $7.7 \cdot 10^{14} \text{ cm}^{-2}/(\text{km s}^{-1} \text{ pc}^{-1})$.

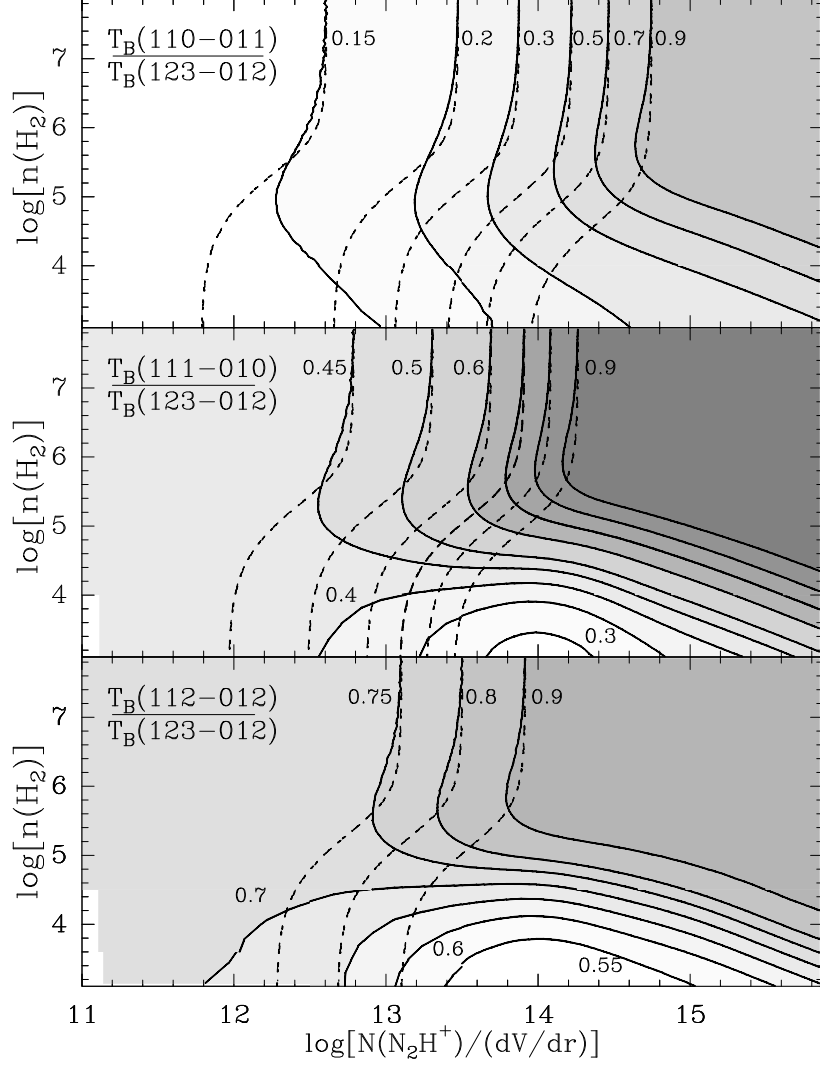


FIG. 5.— Ratio of the brightness temperatures obtained from LTE calculations (long-dashed lines) to those from LVG calculation (continuous lines), for a temperature of $T=10$ K. The reference transition for both calculations is $(JF_1F)=123-012$. The abscissa corresponds to the N_2H^+ column density (from 10^{11} to 10^{16} $\text{cm}^{-2}/(\text{km s}^{-1} \text{ pc}^{-1})$) and the ordinate is the volume density $n(H_2)$ (10^3 - 10^8 cm^{-3}). Under LTE different transitions with the same initial quantum number F have the same brightness temperature. From top to bottom the ratios of transitions with initial quantum number $F = 0, 1, 2$ are shown. These are compared to LVG results for the ratios $T_B(110-011)/T_B(123-012)$, $T_B(111-010)/T_B(123-012)$, and $T_B(112-012)/T_B(123-012)$. Note that for high densities ($n(H_2) > 10^7 \text{ cm}^{-3}$), i.e., thermalized conditions, dotted (LTE) and continuous (LVG) lines converge.

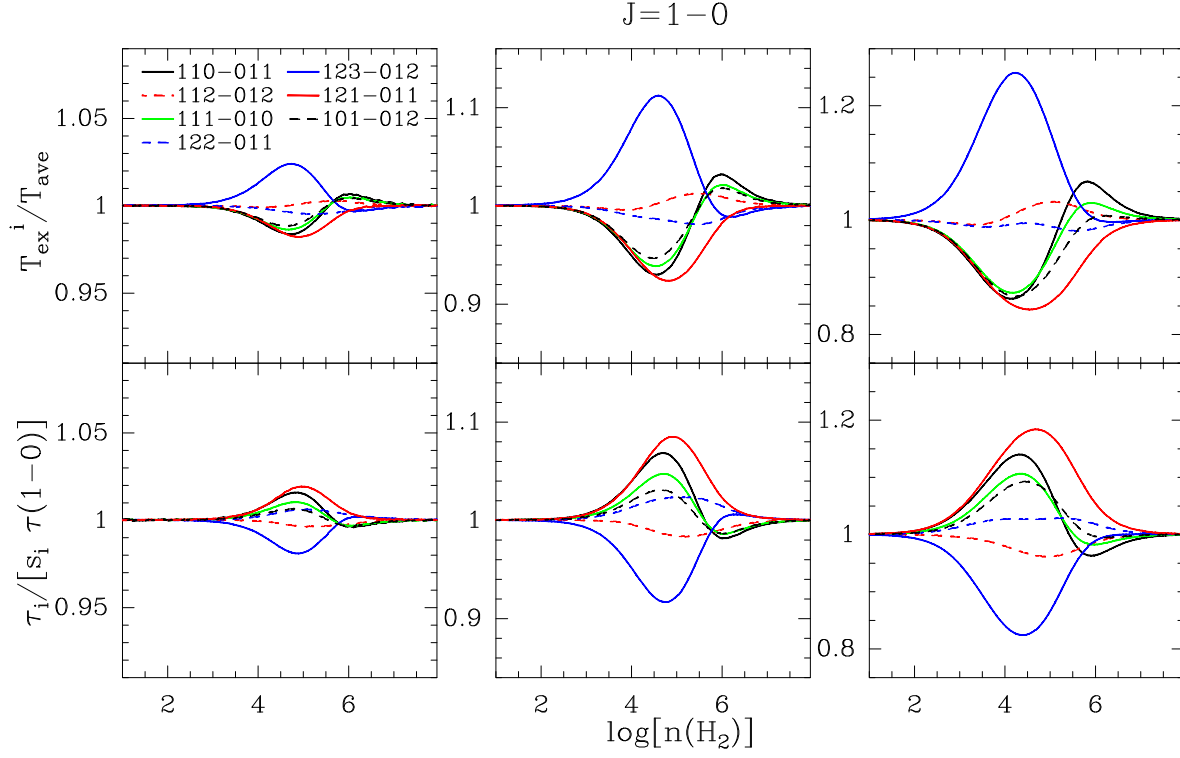


FIG. 6.— Ratio of excitation temperatures and optical depths obtained in the LVG approximation to the corresponding quantities in the LTE limit. The temperature is $T=10\text{K}$ and N_2H^+ column densities are $3.9 \cdot 10^{12}$ (left), $2.5 \cdot 10^{13}$ (center) and $2.0 \cdot 10^{14} \text{ cm}^{-2}/(\text{km s}^{-1} \text{ pc}^{-1})$ (right column). For each set of transitions, the opacities τ_i and the mean excitation temperature T_{ex}^i are obtained by summing over lines with same frequencies and $\tau(1-0)$ and T_{ave} are obtained by summing over all $J=1-0$ hyperfine lines (c.f. eq. 7). Hyperfine set of transitions are referenced using the standard labeling (see Section 2). We see that the variation of the excitation temperatures is anti-correlated with the variation of the opacities.

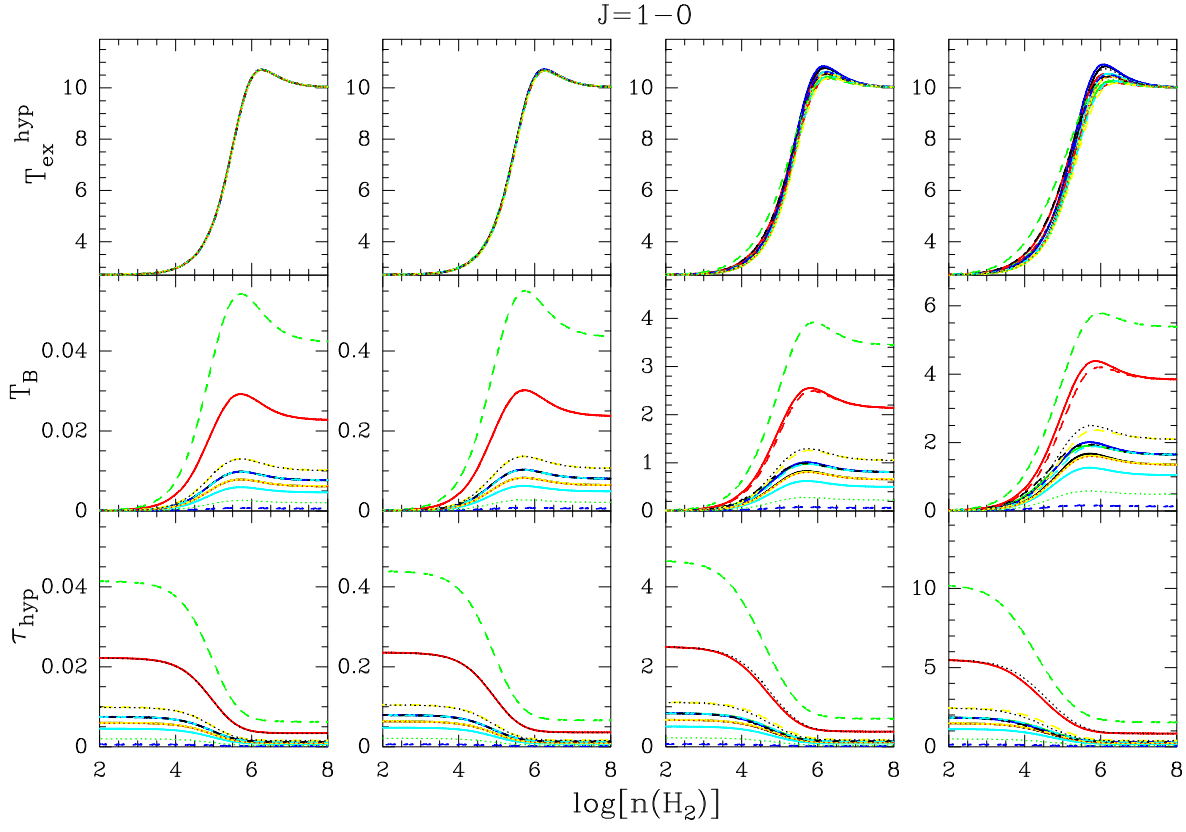


FIG. 7.— Excitation temperatures, opacities and brightness temperatures obtained in the LVG approximation, at $T=10\text{K}$, for the 15 hyperfine components of the $J=1-0$ line. The columns, from left to right, respectively correspond to $N(\text{N}_2\text{H}^+)=2.2 \times 10^{11}$, 2.3×10^{12} , 2.5×10^{13} , and $2.0 \times 10^{14} \text{ cm}^{-2}/(\text{km s}^{-1} \text{ pc}^{-1})$. These column densities correspond to $J=1-0$ total opacities of respectively $\tau(1-0) \sim 0.1$, 1, 10, and 25.

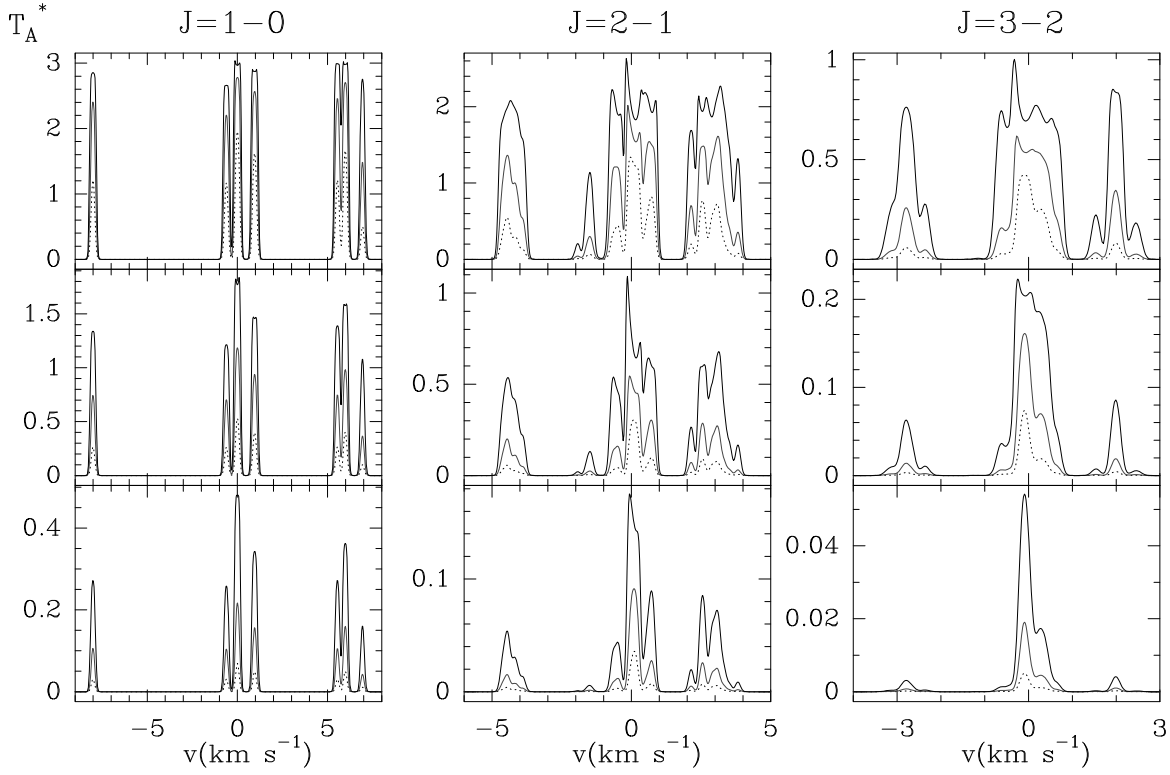


FIG. 8.— Emerging intensities for the $J=1-0$ (left panels), $J=2-1$ (central panels) and $J=3-2$ (right panels) lines of N_2H^+ . The cloud has a uniform volume density, a radius of 3.6×10^{16} cm, a turbulent velocity of 0.1 km s^{-1} , and a kinetic temperature of 10 K. In each box the line profiles are shown for N_2H^+ abundances of 4×10^{-10} (dotted), 1.6×10^{-9} (grey), and 6.4×10^{-9} (solid). From top to bottom the three panels for each transition correspond to volume densities, $n(\text{H}_2)$, of 2.5×10^4 (bottom), 10^5 , and $4 \times 10^5 \text{ cm}^{-3}$ (top).

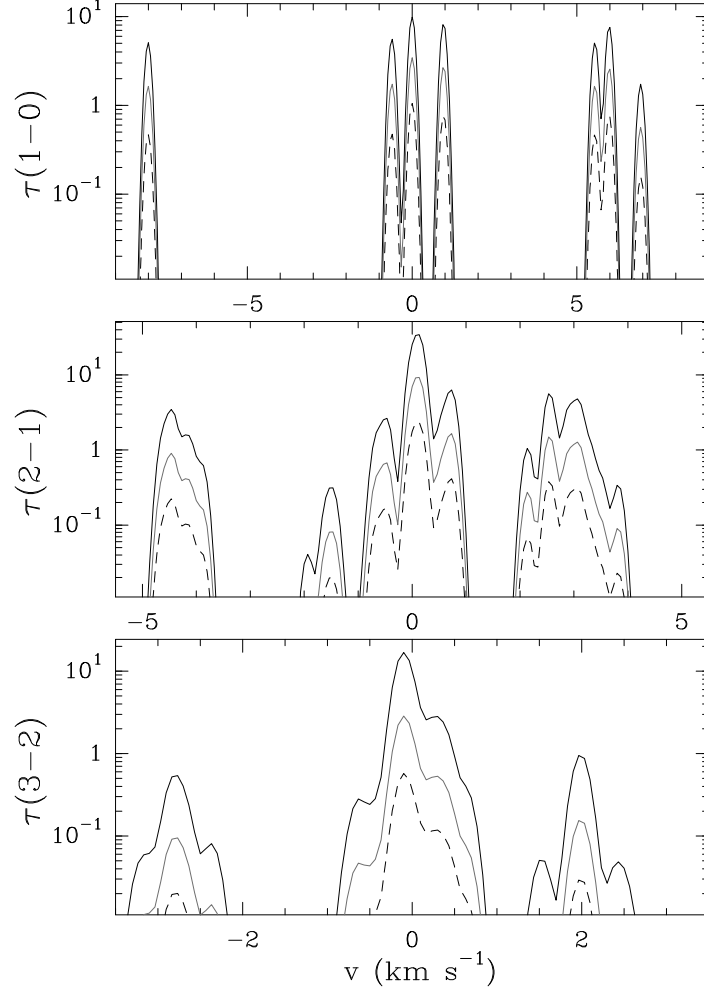


FIG. 9.— Opacities for the $J=1-0$ (top), $J=2-1$ and $J=3-2$ (bottom) lines of N_2H^+ . The cloud has a uniform volume density of 10^5 cm^{-3} , a radius of $3.6 \cdot 10^{16} \text{ cm}$, a turbulent velocity of 0.1 km s^{-1} , and a kinetic temperature of 10 K . N_2H^+ abundance is $4 \cdot 10^{-10}$ (dashed), $1.6 \cdot 10^{-9}$ (gray) and $6.4 \cdot 10^{-9}$ (black).

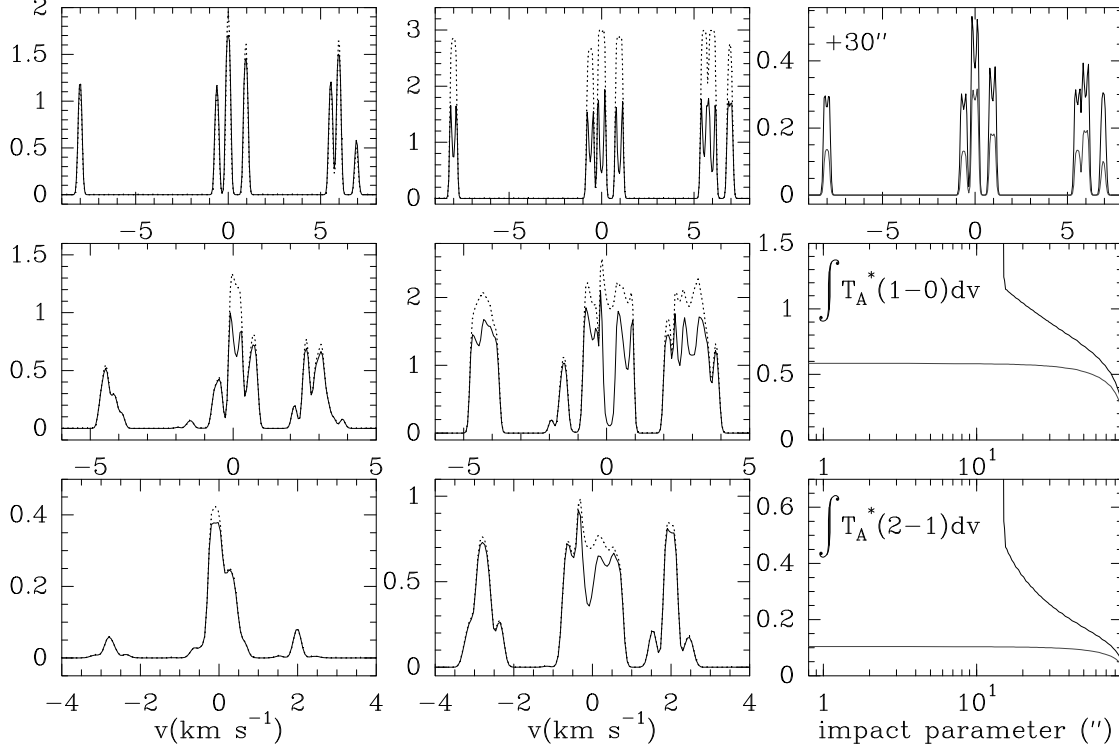


FIG. 10.— Emerging profiles for the $J=1-0$, $J=2-1$ and $J=3-2$ lines of N_2H^+ for a core/envelope geometry (left and central panels). The core has a diameter of $30''$ and a density of $4 \times 10^5 \text{ cm}^{-3}$. The envelope has a diameter of $90''/180''$ and a density of $5 \times 10^4/5 \times 10^3 \text{ cm}^{-3}$ for the left and central panels respectively. The N_2H^+ abundance is $4/64 \times 10^{-10}$ (left/central panels). The kinetic temperature is 10 K and the turbulent velocity is 0.1 km s^{-1} in the core and the envelope. Dotted lines correspond to transitions emerging from the core alone while solid lines correspond to those arising from the core+envelope system. The right panels show the emerging spectrum at an offset position of $30''$ (pure envelope emission corresponds to the gray curve). The effect of the radiative excitation in the envelope due to the photons arising from the core is clearly seen in the two lowest right panels.

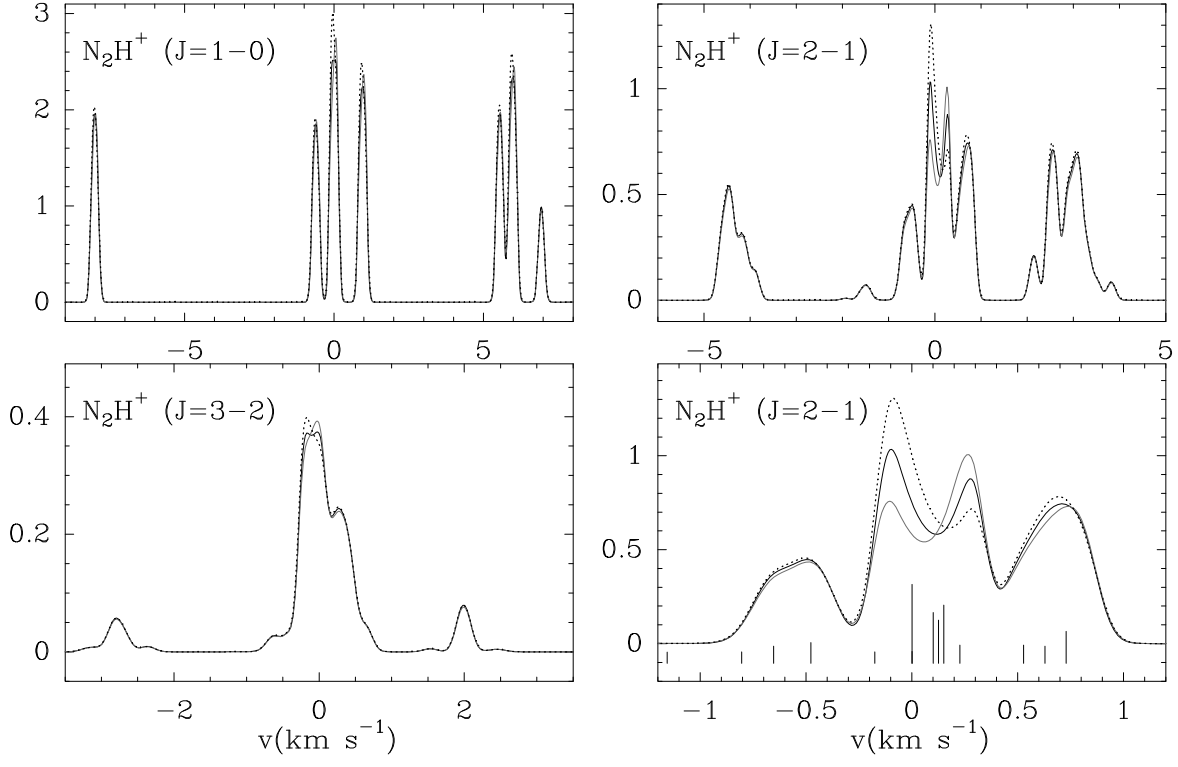


FIG. 11.— Emerging profiles for a cloud with different velocity fields: static (black line), increasing linear function (gray) and decreasing linear function (dotted). The lower right panel shows the central lines of the $J=2-1$ line, with the positions of the individual hyperfine components indicated by lines proportional to their line strength.

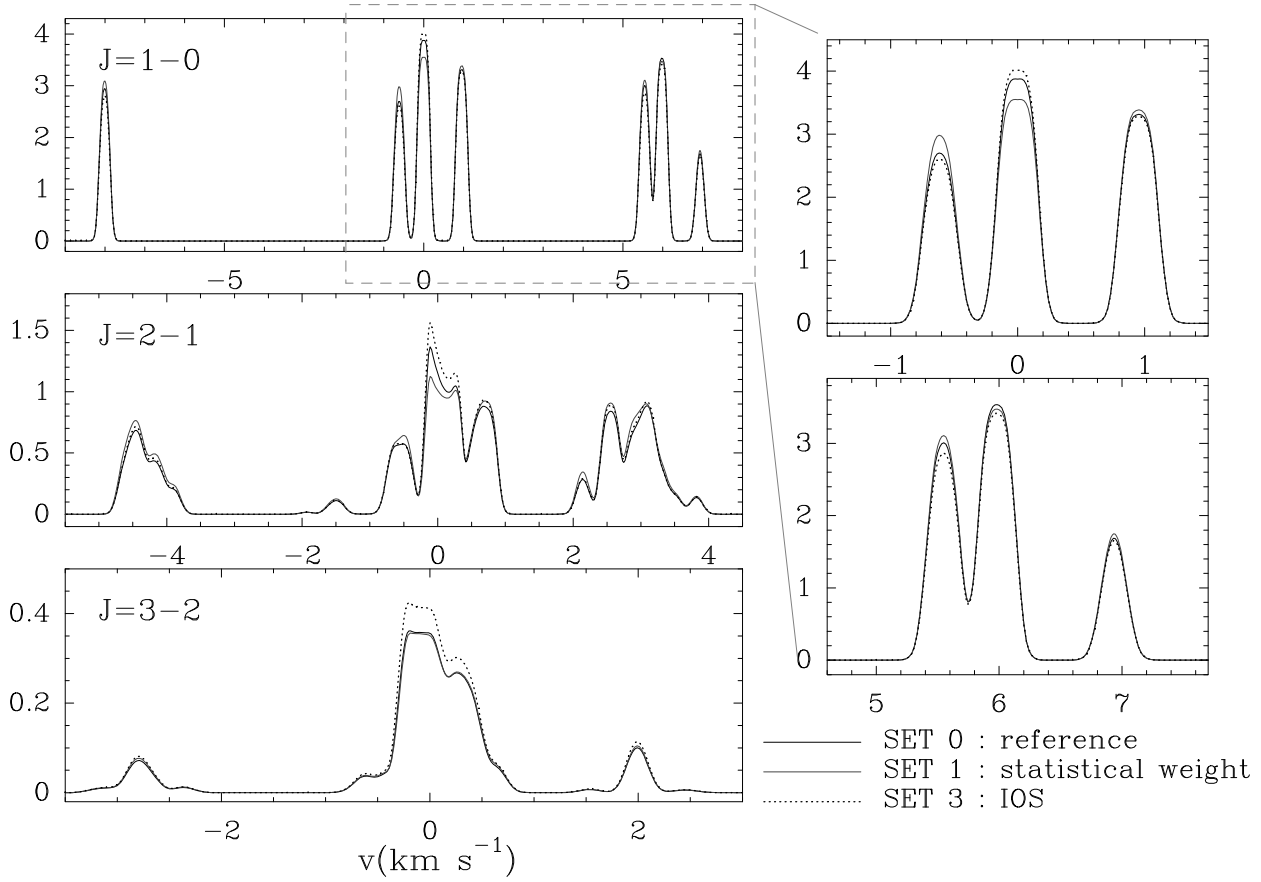


FIG. 12.— $J=1-0$, $2-1$ and $3-2$ emerging profiles (left column) for a cloud at $T_K = 10\text{K}$, $n(\text{H}_2) = 2 \cdot 10^5 \text{ cm}^{-3}$ and $X(\text{N}_2\text{H}^+) = 5 \cdot 10^{-10}$. Two approximations for the hyperfine collisional rate coefficients (see text) are compared to the set of reference (black solid line). The first consist of rates proportional to statistical weights (gray solid lines) and the second is based on the IOS approximation (dashed lines). The right column corresponds to a blow-up of the $J=1-0$ hyperfine lines.

$J=1-0$

